THE ROLE OF CONSTRAINTS IN FUTURE MOTION SYSTEMS

T. Raste[1]

[1] Continental, Guerickestr. 7, 60488 Frankfurt/Main, Germany,
thomas.raste@continental-corporation.com, www.continental.com

Keywords: Motion Control, Model Predictive Control, Torque Vectoring, Energy Recuperation.

ABSTRACT

The vehicle motion is affected by a number of constraints: the performance limits of the actuators, fault tolerant control reconfiguration and safety limits as well as energy-related dynamic control allocation. Tire-road friction circles constraining the admissible forces at the wheels are approximated by polytopes. These factors are systematically taken into account by equality and inequality constraints of a Model Predictive Controller (MPC) at chassis level. Wheel modules receive the incoming stream of chassis requests and generate a stream of requests to the actuators. A wheel module MPC framework at the front axle is able to optimally split the wheel braking torque among the redundant actuators, while providing anti-lock braking features by wheel slip regulation. This approach offers fast transient response, without compromising the energy recuperation efficiency of the electric motors taking different dynamic authorities of friction brake and electric motor into account.

1 INTRODUCTION

Future motion systems for autonomous and manual driving should meet increased requirements for energy efficiency, safety and driving dynamics. Early motion control concepts have been described in [4] and [12]. First set-based methods have been successfully applied in automotive [6], [16] and flight control [9], [10]. Recent publications combine sets with model predictive control for collision avoidance in [1] and [17] or use reachable sets for collision-free automated driving [2]. In future motion systems an increasing number of constraints have to be considered in real-time during constraint optimization. Table 1 gives a non-exhaustive overview of the role of constraints in motion systems.

Role	Constraint	Example
Actuator limitation	Bounds	Electric motor torque
Control allocation	Equality constraints (or inequality constraints)	Torque vectoring, recuperation torque blending
Variant management	Equality constraints	Manual front axle steering
Admissible controls	Polytopes	Tire force limit (Kamm's circle)
Attainable forces	Zonotopes	Total force limit (g-g Diagram)
Vehicle stabilization	Polytopes	Stability envelope
Cross redundancy	Inequality constraints	Actuator fault tolerance
Freespace driving	Intersection of reachable set with collision free area	Occupancy prediction
Collision avoidance	Non-convex	Intersections (Mixed-Integer Programming)

Table 1: Role of constraints in motion systems.

2 FUTURE MOTION SYSTEM

The Motion System is depicted in fig. 1 and complements seamlessly the Autonomous Driving software and hardware stack. The motion system modules are aligned along the chain of effects starting from vehicle level via chassis level down to the wheel level. This cascaded, modular structure reflects the interconnections in the motion domain: Horizontal vehicle motion is determined by the wheel steering angles and wheel moments at any given time, which also determine the horizontal tire forces. The chassis links the wheels with the vehicle body.

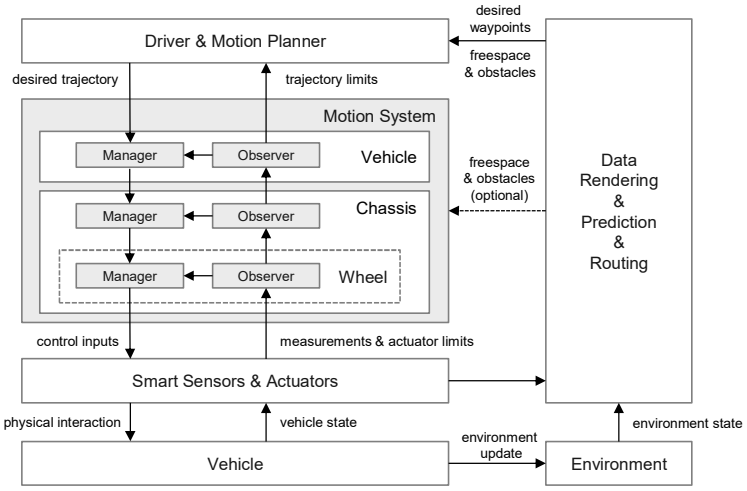

Figure 1: Future Motion System.

Observer functions provide information for the own and the higher level and coordinate limits received from the lower level. Manager functions place service requests to control the respective lower level. Candidates for request variables are curvature/acceleration, speed/torque, position/force or only a subset of them. It is agreed upon that requests to more than one level below are not possible for the requesting manager

3 MODEL PREDICTIVE TRACKING CONTROL

The control concept illustrated in fig. 2 shows the interconnections of the managers through the levels on the example of an electric vehicle with six individually controllable actuators. There are friction brakes at each wheel and electric motors at each front wheel available for motion control. Steering is considered to be manually actuated by the driver, but a position tracking control like in [13] or [15] can be integrated straightforward.

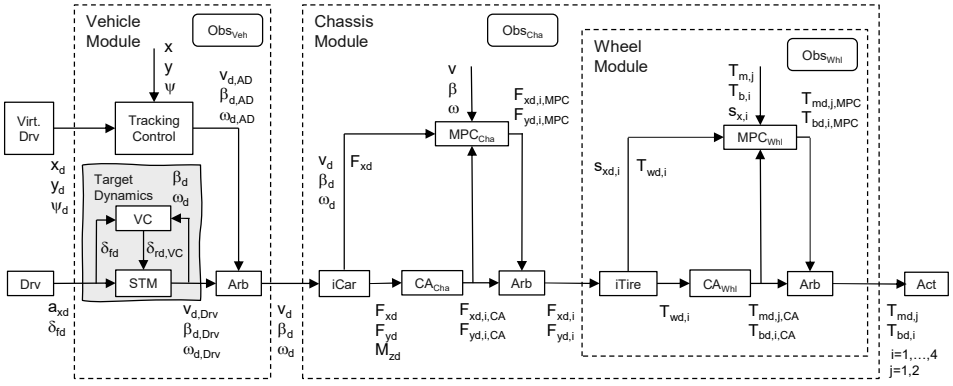

Figure 2: Motion control concept with single track model (STM), virtual rear steer angle control (VC), static control allocation (CA), inverse vehicle model (iCar), inverse tire model (iTire), model predictive control (MPC), observers (Obs), actuators (Act), arbitration (Arb), driver (Drv) and assisted or autonomous driver (Virt. Drv).

The motion control concept shown in fig. 2 includes feedforward and feedback control parts. Feedforward control ensures customizable target vehicle dynamics by providing a desired vehicle state with speed v_d, side slip angle β_d and yaw rate ω_d. The target dynamics is translated into total longitudinal and lateral forces F_{xd}, F_{yd} respectively and yaw moment M_{zd}. The chassis MPC tracks the desired vehicle state and ensures agility and stability by torque vectoring with dynamic control allocation of the total forces and moment to eight horizontal wheel corner forces $F_{xd,i}$, $F_{yd,i}$, i=1,…,4. Inverse tire models determine for each wheel the desired longitudinal wheel slip $s_{xd,i}$ and wheel torque $T_{wd,i}$. The wheel MPCs track the torque and slip and dynamically allocate the torques at the front wheels to the electric motors and friction brakes to maximize energy efficiency by recuperation.

3.1 Problem Formulation

Model predictive control is an optimal control strategy that uses a model of the system to obtain an optimal control sequence by minimizing an objective function, [7]. At each sampling instant, the model is used to predict the behavior of the system over a prediction horizon of N sampling intervals. We denote with u_j, x_j input and state vectors at sample instants $j = k, k+1,\ldots, k+N-1$ predicted at sample time k. To reduce computational effort, it may be advisable to optimize the input over a shorter control horizon of $M < N$ sampling intervals and fix the inputs to constant values in the remaining intervals. This policy is referred to as “move blocking”, cf. [8]. The MPC optimization approach used in the present motion control concept comprises the following generic form

$$\min_{u_{ck},\ldots,u_{ck+M-1},\varepsilon_k} \quad J_T(x_j,u_j) + P\varepsilon_k^2 \tag{1a}$$

$$\text{subject to } x_{j+1} = A_j x_j + B_j u_j + h_{xj} \tag{1b}$$

$$y_j = C_j x_j + D_j u_j + h_{yj} \tag{1c}$$

$$w_j = C_{wj} x_j + D_{wj} u_j + \varepsilon_k V_w \tag{1d}$$

$$[u_k^T,\ldots,u_{k+N-1}^T]^T = (M \otimes I_m)\,[u_{ck}^T,\ldots,u_{ck+M-1}^T]^T \tag{1e}$$

$$x_0 = x_k \tag{1f}$$

$$u_{min} \le u_j \le u_{max} \tag{1g}$$

$$y_{min} - \varepsilon_k V_{y,min} \le y_j \le y_{max} + \varepsilon_k V_{y,max} \tag{1h}$$

$$\Delta u_{min} - \varepsilon_k V_{\Delta u,min} \le \Delta u_j \le \Delta u_{max} + \varepsilon_k V_{\Delta u,max} \tag{1i}$$

$$H_{xj} x_j + H_{uj} u_j \le b_{Hj} + \varepsilon_k V_H \tag{1j}$$

$$0 \le \varepsilon_k \tag{1k}$$

$$\forall j \in \{k,\ldots,k+N-1\} \tag{1l}$$

The overall cost function is divided into a trajectory tracking part J_T and a slack variable ε penalized with weighting P. The slack is here declared scalar, but to ensure feasibility of the optimization problem a vectorized slack could be more appropriate. The cost function used for target tracking is quadratic and allows penalization of the output error, input error and input rate by the symmetric positive semidefinite weighting matrices Q, R and R_Δ

$$J_T = \sum_{j=k}^{k+N} ((y_j - y_{dj})^T Q (y_j - y_{dj})) + \sum_{j=k}^{k+N-1} ((u_j - u_{dj})^T R (u_j - u_{dj}) + \Delta u_j^T R_\Delta \Delta u_j) \tag{2}$$

The constraints of the MPC problem (1) can be divided into equality constraints and inequality constraints. The first three equality constraints are the vehicle dynamics state and output model in affine form and a general soft constraint as a linear combination of state and input softened by the slack variable. The target vector w is either zero or must be provided externally. The next equality constraint is used to realize a control horizon shorter than the prediction horizon by move blocking. The matrix M determines the blocking scheme and the operator symbol is the Kronecker product. The last equality constraint maps the initial state to the current state of the sampling period. The inequality constraints determine the bounds for the input u, output y and input rate Δu. The latter two are softened to ensure feasibility of the optimization. A polytopic set constraint optionally softened and the non-negativeness of the slack variable are the remaining inequality constraints

3.2 Chassis and Wheel Model

The chassis model is based on a twin track vehicle model and the wheel models include a first order actuator dynamics and the wheel slip dynamics. The models are derived from the quantities shown in fig. 3.

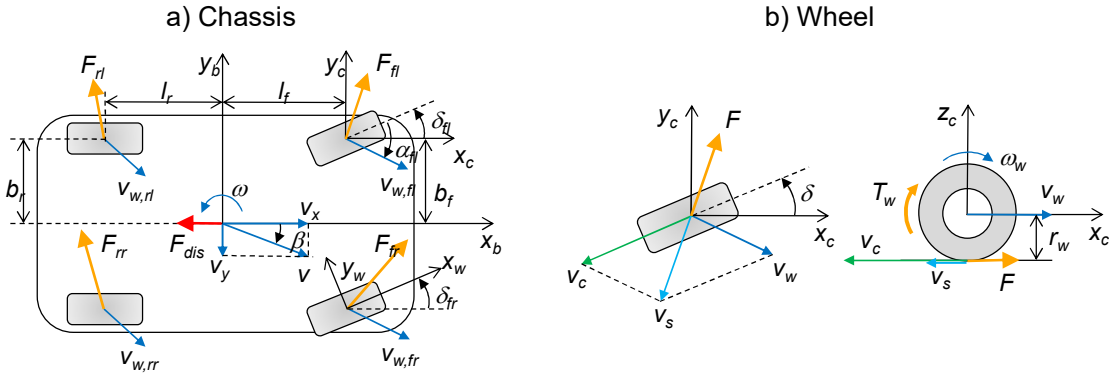

Figure 3: Geometric, kinematic and dynamic quantities of chassis and wheel model.

The chassis dynamics is given with vehicle mass m, inertia J_z and air drag constant k_x by the nonlinear equations

$$d/dt\, v_x = v_y\, \omega - k_x/m\, v_x^2 + 1/m\, F_x, \tag{3a}$$
$$d/dt\, v_y = -\, v_x\, \omega + 1/m\, F_y, \tag{3b}$$
$$d/dt\, \omega = 1/J_z\, M_z, \tag{3c}$$

together with equation (4a) including the 3 x 8 matrix G relating the total forces and moment with the corner forces

$$[F_x\, F_y\, M_z]^T = G\, u, \tag{4a}$$
$$u = [F_{xd,fl,MPC},\, F_{yd,fl,MPC},\, \ldots,\, F_{xd,rr,MPC},\, F_{yd,rr,MPC}]^T, \tag{4b}$$
$$G = [1\ 0\ 1\ 0\ 1\ 0\ 1\ 0;\ 0\ 1\ 0\ 1\ 0\ 1\ 0\ 1;\ -b_f\ l_f\ b_f\ l_f\ -b_r\ -l_r\ b_r\ -l_r] \tag{4c}$$

The model (3) and (4) is linearized along the desired state and input before used in the chassis MPC equation (1b) and (1c). The wheel model is linear time variant with state variables electric motor torque T_m, friction brake torque T_b and longitudinal wheel slip s_x given with actor time constants T_{1m} and T_{1b}, wheel radius r_w, tire inertia J_w, tire force stiffness k_{Fx} and wheel longitudinal velocity v_{wx} by

$$d/dt\, T_m = -\, 1/T_{1m}\, T_m + 1/T_{1m}\, T_{md,MPC}, \tag{5a}$$
$$d/dt\, T_b = -\, 1/T_{1b}\, T_b + 1/T_{1b}\, T_{bd,MPC}, \tag{5b}$$
$$d/dt\, s_x = -r_w^2 k_{Fx}/(J_w\, v_{wx})\, s_x + r_w/(J_w\, v_{wx})\, T_w, \tag{5c}$$
$$T_w = T_m + T_b. \tag{5d}$$

The rear wheel models do not include (5a) and no electric motor torque T_m in the output equation (5d).

3.3 Set-based Constraints Calculation

Sets appear naturally when constraints are considered in control system design [5]. We denote sets with bold letters and need three type of convex sets: intervals, polytopes and zonotopes. The calculation of the sets is done with the Matlab toolbox CORA [3]. An interval is defined by

$$\boldsymbol{I} := \{x \in \mathbb{R}^n \mid x_{i,min} \le x \le x_{i,max}\ \forall i = 1, \ldots, n\} \tag{6}$$

with lower bound $x_{i,min}$ and upper bound $x_{i,max}$. The above constraints (1g-i) are all interval constraints. The speed dependent bounds for the electric motor torques are illustrated in fig. 4.

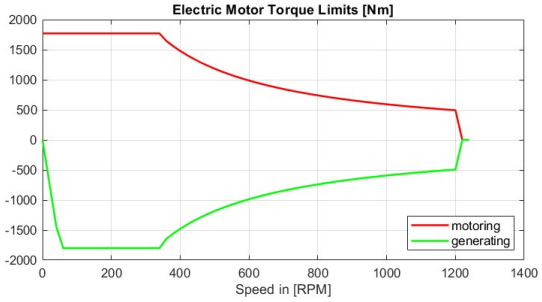

Figure 4: Speed dependent bounds for the electric motor torques.

A polytope in halfspace representation is given by

$$\boldsymbol{P} := \{x \in \mathbb{R}^n \mid Hx \leq b\}, x \in \mathbb{R}^{q\,x\,n}, b \in \mathbb{R}^q \tag{7}$$

where the matrix H collects the normal vectors of q hyperplanes in their rows and vector b collects the scalar products of x with the normal vectors of each row in H. The polytope is the nonempty intersection of q halfspaces. The polytope constraints shown in fig. 5 limit the state and input of the chassis MPC. The set of admissible forces are the intersections of the upper bound halfspaces with the friction circles. The latter are calculated utilizing estimated vertical forces and tire-road friction value. Road Condition Observers provide friction estimates, cf. [14].

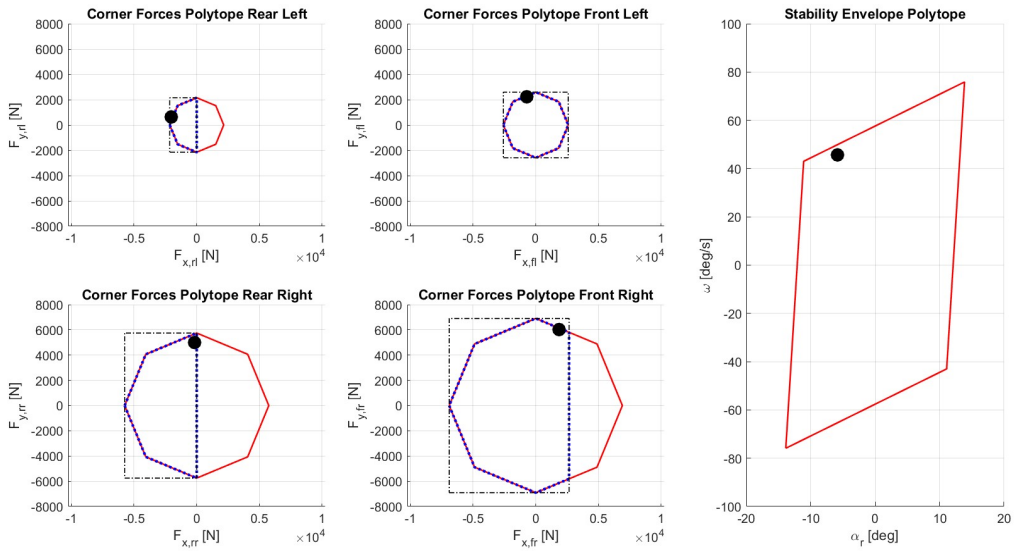

Figure 5: Polytope constraints limiting state and input of the chassis MPC. Friction circles in solid (red), admissible wheel forces in dashed (blue) and an interval approximation in dashed-dotted (black). All polytopes are determined for the maneuver shown in fig. 7 at t = 0.3s with the filled circles indicating the actual vehicle dynamics values.

A zonotope is the image of a hypercube under an affine projection and is defined by

$$\boldsymbol{Z} := \{x \in \mathbb{R}^n \mid x = x_0 + \sum_{i=1}^{p} z^{(i)} v_i, v_i \in [-1, 1]\} \tag{8}$$

where x_0 is the center and $z^{(i)}$ are the generators. The zonotope describes the set of attainable total forces and yaw moment and can be calculated according to [9]. At first an eight-dimensional interval set is built from the corner forces intervals shown in fig. 5,

$$\boldsymbol{I}(u_{min},\, u_{max}), \tag{9a}$$
$$u_{min} = 0.5\,[F_{x,fl,min},\, F_{y,fl,min},\, \ldots,\, F_{x,fl,min},\, F_{y,fl,min}]^T \tag{9b}$$
$$u_{max} = 0.5\,[F_{x,fl,max},\, F_{y,fl,max},\, \ldots,\, F_{x,fl,max},\, F_{y,fl,max}]^T \tag{9c}$$

The center x_0 and the generators $z^{(i)}$ of the zonotope (8) is calculated from the control limits (9b,c) and matrix (4c) using the center function from CORA and $g^{(i)}$ the i-th column of G,

$$x_0 = 2\,G\,u_0,\; u_0 = \text{center}(\,\boldsymbol{I}(u_{min},\, u_{max})\,), \tag{10}$$
$$z^{(i)} = g^{(i)}\,(u_{max,i} - u_{min,i}),\; i = 1,\, \ldots,\, 8,$$

The result is shown in fig. 6. It is worth to note that the zonotope is an over-approximation. For comparison the Minkowski sum of the corner polytopes of admissible forces representing the limits of longitudinal and lateral total forces is displayed (i.e. g-g diagram when scaled with vehicle mass).

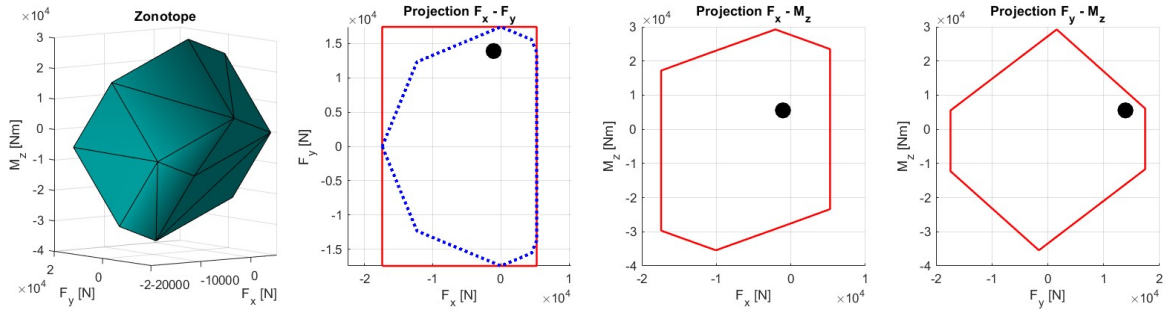

Figure 6: Three-dimensional zonotope as the set of attainable total forces and yaw moment and respective projections in solid (red). Set of attainable longitudinal and lateral total force in dashed (blue) calculated with Minkowski sum of admissible corner force polytopes. The zonotope is determined for the maneuver shown in fig. 7 at t = 0.3s with the filled circles indicating the actual vehicle dynamics values

4 SIMULATION RESULTS

Simulation results confirm the validity of the motion control concept, which will be explained and illustrated on the basis of the requested and actual vehicle dynamics data. In all simulations, the sample time of the chassis MPC is T_s=10ms and the prediction and control horizon is equal with N=3 and M=3. The four wheel MPC's sample times are 2ms and the prediction and control horizons are N=5 and M=3 respectively. The qpOASES solver described in [11] is used to provide the solution of the quadratic program (1).

The first test case is a collision avoidance maneuver at the limits of handling at 80 km/h illustrating the torque vectoring capability to improve agility and at the same time stability, cf. figure 7. The rear steer angle is purely virtual and controls the yaw rate response of the virtual single track model in the vehicle manager. In order to follow the high-dynamic yaw request closely the chassis MPC allocates the forces accordingly taking a high rear side slip angle into account. The dynamics is quite impressive, a 3m lateral displacement is reached after 1s. This is only possible, because the stability envelope allows high transient yaw rates.

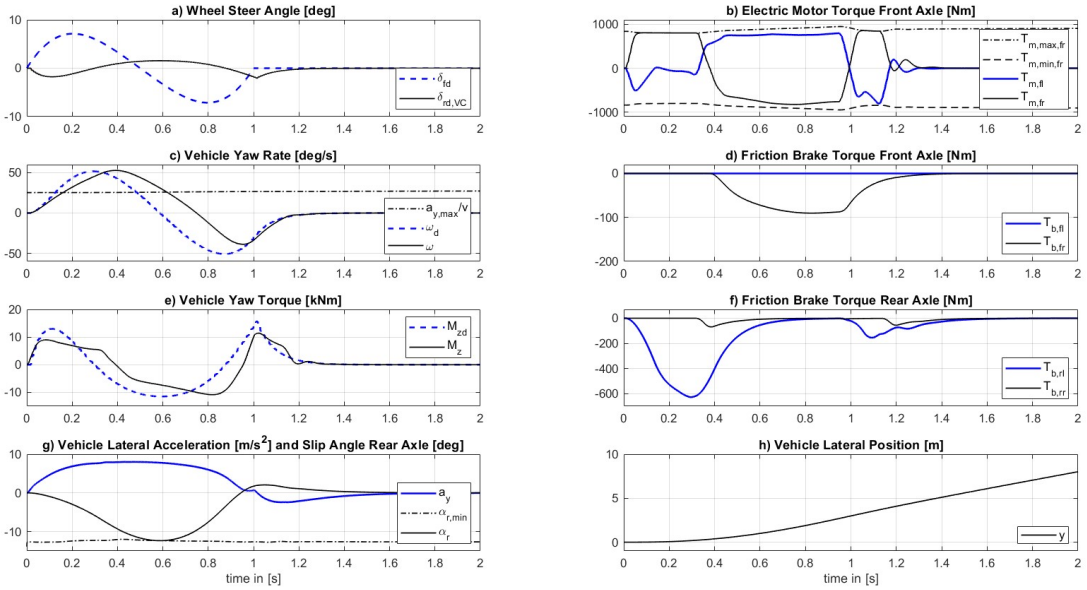

Figure 7: Simulation of a collision avoidance maneuver at the limits of handling.

The second test case is a courageous straight-ahead braking test to visualize the front-to-rear torque vectoring by the chassis manager MPC and a brake torque blending by the two wheel MPCs at the front axle, see figure 8. The maneuver is continuously straight and symmetric, such that only the left side is visualized. The static control allocation ensures prioritization of the front axle with the electric motors but does not take any constraints into account. This is the task of the chassis MPC, which dynamically allocates the forces due to its friction limits trying to track the requested deceleration. The front wheel MPCs perform a dynamic control allocation to blend between electric motor and friction brake torques when the motors reach their limits during the maximum power phase and near standstill. In the force saturation phase all wheel MPCs perform slip control to avoid wheel locking, at the front wheels even during blending

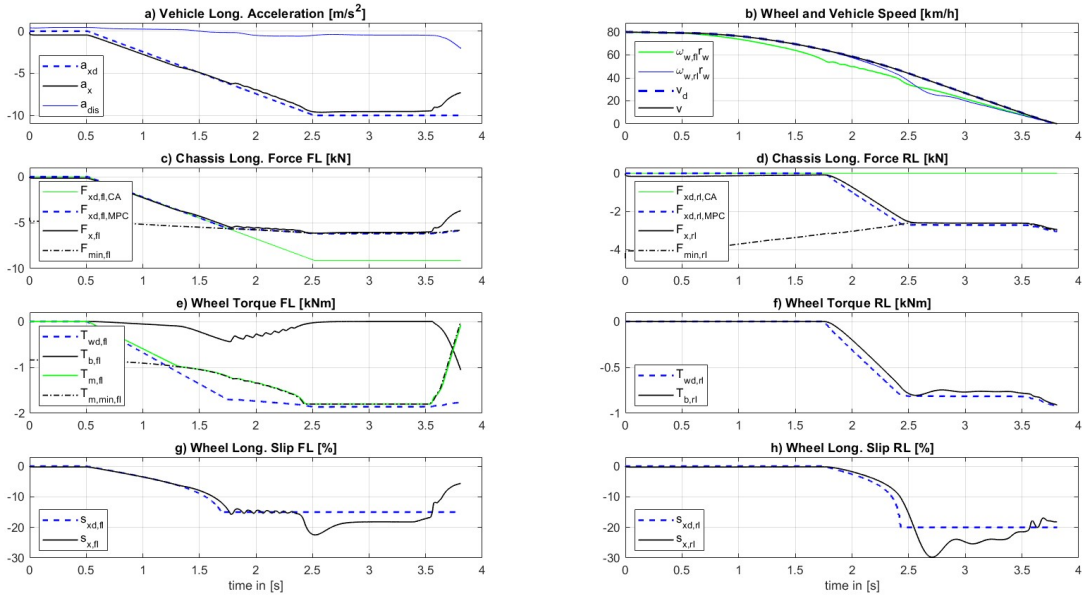

Figure 8: Simulation of a straight-ahead braking maneuver with energy recuperation prioritization, c) and d) torque vectoring between front and rear axle, e) torque blending at front axle with maximum regenerative braking torque limit exploited, g) and h) wheel slip regulation.

The last maneuver is the same straight ahead braking with fixed steering at zero as in figure 8, but with a failure of the front left friction brake actuator, see figure 9. At the same time the electric motors are limited at -500 Nm due to nearly full battery. This situation would produce a dangerous disturbance yaw torque leading to immediately spinning of the vehicle without control. With motion control the situation is controllable by the driver at any time. The strategy is to reduce the force limits at the remaining healthy corners to provide stability. The amount of reduction was chosen to minimize lateral motion. With this simple measure the chassis MPC is able to re-allocate the braking forces in a way that the disturbance yaw torque is counteracted for and at the same time the driver braking request is satisfied, but at a lower level compared to the fault free case

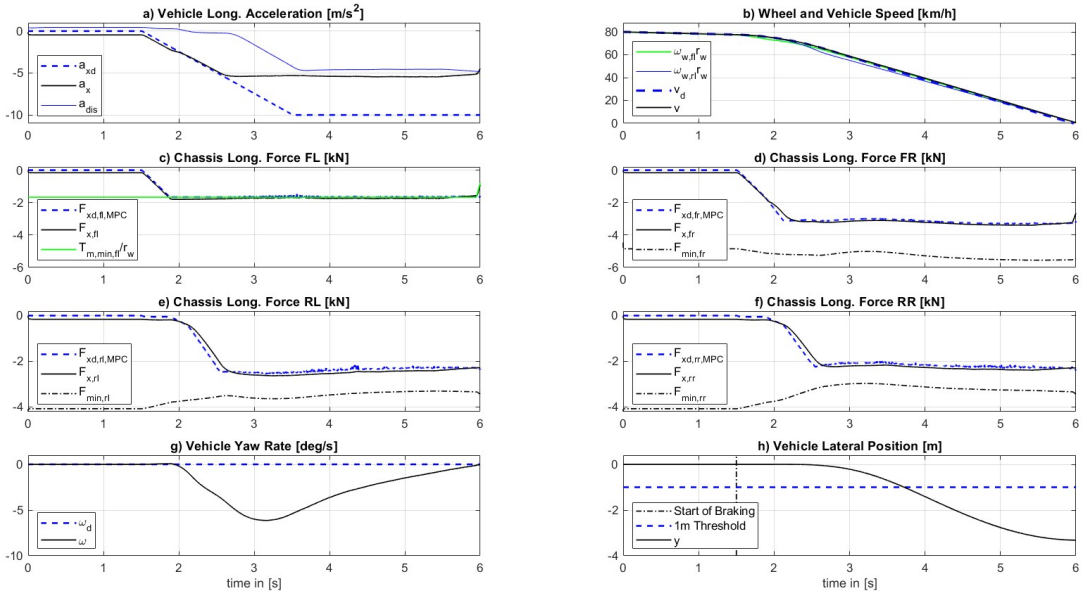

Figure 9: Simulation of actuator failure, a) loss of deceleration considered in reference velocity by disturbance estimation, c) friction brake front left failure, electric motor limited, d) - f) vehicle stability ensured by reduction of polytope force constraints at rear axle to 70% and at front right wheel to 60%, h) path deviation is controllable by the driver.

5 CONCLUSIONS

In this paper we proposed a model predictive controller (MPC) cascade for managing the complexity of future motion systems. The goal of such modular controller framework is to provide an appropriate interface for autonomous and manual driving, maximizing energy recuperation, improving agility and stability and ensuring safety by a central redundancy management in case of actuator failures. The vehicle motion is predicted using a twin track dynamic vehicle model and wheel models. The latter encapsulate the dynamics of the wheel slip and actuators. The constraints include polytopic approximations of the friction circles and a stability envelope. All constraints are based on coordinated limits propagated through the cascade in an upstream direction from smart actuators to the vehicle level. The MPCs were formulated as convex optimization by linearizing the models around requests from higher levels and including the requests in the cost function for tracking. As future work, we would like to investigate a greater portfolio of smart actuators including vertical motion for the next generation electric vehicles. Finally, we would like to evaluate adaptability of the vehicle capabilities over the whole lifecycle using our high-performance computing platforms with edge and cloud connectivity

REFERENCES

[1] B. Alrifaee, Networked Model Predictive Control for Vehicle Collision Avoidance, *Ph.D. Thesis,* RWTH Aachen University, 2017.

[2] M. Althoff, S. Magdici, Set-Based Prediction of Traffic Participants on Arbitrary Road Networks, *IEEE Transactions on Intelligent Vehicles,* **Volume 1, Issue 2**, 2016, pp. 187-202.

[3] M. Althoff, N. Kochdumper, M. Wetzlinger, CORA Manual (tumcps.github.io/CORA/), 2020.

[4] J. Andreasson, On Generic Road Vehicle Motion Modelling and Control, *Ph.D. Thesis,* KTH Stockholm University, 2007.

[5] F. Blanchini, S. Miani, Set-Theoretic Methods in Control, Springer, Cham, 2015.

[6] C. G. Bobier, A Phase Portrait Approach to Vehicle Stabilization and Envelope Control, *Ph.D. Thesis,* Stanford University, 2012.

[7] F. Borelli, A. Bemporad, M. Morari, Predictive Control for Linear and Hybrid Systems, University Press, Cambridge, 2017.

[8] R. Cagienard, P. Grieder, E. C. Kerrigan, M. Morari, Move blocking strategies in receding horizon control, *Journal of Process Control,* **17**, 2007, pp. 563-570.

[9] M. Demenkov, Geometric algorithms for input constrained systems with application to flight control, *Ph.D. Thesis,* Leicester University, 2007.

[10] W. Durham, K. A. Bordignon, R. Beck, Aircraft Control Allocation, John Wiley & Sons, Chichester, 2017.

[11] H. J. Ferreau, An Online Active Set Strategy for Fast Solution of Parametric Quadratic Programs with Applications to Predictive Engine Control, *Diploma Thesis,* Ruprecht-Karls Heidelberg University, 2006.

[12] M. Jonasson, Exploiting individual wheel actuators to enhance vehicle dynamics and safety in electric vehicles, *Ph.D. Thesis,* KTH Stockholm University, 2009.

[13] T. Raste, A. Tarraf, Flachheitsbasierte Trajektoriengenerierung und Folgeregelung mit modellprädiktiver und modellfreier Regelung, *VDI/VDE Fachtagung AUTOREG, Berlin, Germany, June 5th – 6th 2017,* VDI-Berichte, Band 2292, 2017, pp. 319-324.

[14] T. Raste, P. Lauer, B. Hartmann, Development of a Road Condition Observer for the "Vehicle Motion Control" Project, *Int. μ-Symposium 2018 Brake Conference (Ed. R.Mayer.), Bad Neuenahr, Germany, October 26th 2018,* Springer Vieweg, 2019, pp. 127-142.

[15] T. Raste, P. Lauer, Bewegungssteuerung für ein Robo-Taxi mit Symmetrie in Antrieb und Lenkung, *VDI/VDE Fachtagung AUTOREG, Mannheim, Germany, July 2th – 3th 2019,* doi 10.51202/9783181023495, pp. 129-144.

[16] C. W. Satzger, Predictive Braking Control with Hybrid Actuators, *Ph.D. Thesis,* Erlangen: FAU University Press, 2017.

[17] L. Svensson, M. Bujarbaruah, N. R. Kapania, M. Törngren, Adaptive Trajectory Planning and Optimization at Limits of Handling, *arXiv:1903.04240v4 [cs.RO] 10 Dec 2019.*